Chiral charge order in the superconductor 2H-TaS$_2$

I Guillamón[1,2]**, H Suderow**[1,6]**, J G Rodrigo**[1]**, S Vieira**[1]**,
P Rodière**[3]**, L Cario**[4]**, E Navarro-Moratalla**[5]**, C Martí-Gastaldo**[5]
and E Coronado[5]

[1] Laboratorio de Bajas Temperaturas, Departamento de Física de la Materia
Condensada, Instituto de Ciencia de Materiales Nicolás Cabrera,
Facultad de Ciencias, Universidad Autónoma de Madrid, E-28049 Madrid,
Spain
[2] H H Wills Physics Laboratory, University of Bristol, Tyndall Avenue,
Bristol BS8 1TL, UK
[3] Institut Néel, CNRS / UJF, 25, Av. des Martyrs, BP166, 38042 Grenoble
Cedex 9, France
[4] Institut des Matériaux Jean Rouxel (IMN), Université de Nantes–CNRS,
2 rue de la Houssiniére, BP 32229, 44322 Nantes Cedex 03, France
[5] Instituto de Ciencia Molecular (ICMol), Universidad de Valencia,
Catedrático José Beltrán 2, 46980 Paterna, Spain
E-mail: hermann.suderow@uam.es

Abstract. We observed chiral charge order in the superconductor 2H-TaS$_2$
using scanning tunneling microscopy and spectroscopy at 0.1 K. Topographic
images show hexagonal atomic lattice and charge density wave (CDW) with
clockwise and counterclockwise charge modulations. Tunneling spectroscopy
reveals the superconducting density of states, disappearing at $T_c = 1.75$ K and
showing a wide distribution of values of the superconducting gap, centered
around $\Delta = 0.28$ meV.

[6] Author to whom any correspondence should be addressed.

IOP Institute of Physics ⏀ DEUTSCHE PHYSIKALISCHE GESELLSCHAFT

Contents

1. Introduction

Since the suggestion by Anderson and Blount [1] that charge order may appear in metals and superconductors, the size and anisotropy of charge density wave (CDW) modulations has been an intensely debated issue [2, 3]. Layered compounds, such as hexagonal bilayer stackings of dichalcogenides, named 2H, have received attention because the charge order is only partial and clean metallic behavior is ubiquitously observed. In the 2H series of $TaSe_2$, TaS_2, $NbSe_2$ and NbS_2, the critical temperature of the CDW decreases from around 120 K in 2H-$TaSe_2$, to 80 K in 2H-TaS_2, down to 30 K in 2H-$NbSe_2$ and finally no CDW in 2H-NbS_2 [4, 5]. Superconductivity coexists with CDW, with a superconducting critical temperature T_c that increases from around 0.2 K in 2H-$TaSe_2$ up to 7.2 and 6 K in 2H-$NbSe_2$ and 2H-NbS_2, respectively. Generally, it is believed that their mutual interaction is competitive, as charge order usually drives towards insulating behavior and superconductivity towards perfect conductance. However, evidence for cooperative interactions, which actually shape the form of the gap over the Fermi surface, have been found in angular resolved photoemission [2]. CDW significantly shapes the anisotropy of the superconducting properties of the compound 2H-$NbSe_2$, producing vortex cores with a star-shaped cross section, instead of the tubular cores expected in a simple isotropic s-wave superconductor [6–9].

The Fermi surface of all four 2H compounds (2H-$TaSe_2$, 2H-TaS_2, 2H-$NbSe_2$ and 2H-NbS_2) consists essentially of warped tubes deriving from the d-electrons of the transition metal, with a strong hybridization to the p-electrons of the chalcogen [10, 11]. Calculations found that, generally, p-electron-derived bands of the chalcogens do not cross the Fermi level, with the important exception of 2H-$NbSe_2$, where they form a small three-dimensional (3D) pocket [12, 13]. The charge order properties have been studied in the whole series, although usually at temperatures well above liquid helium (see, e.g., [14]). Only the superconducting properties 2H-$NbSe_2$ and 2H-NbS_2 have been analyzed in some detail, finding peculiar multigap superconducting behavior [9, 15–19].

On the other hand, in the related semimetallic compound 1T-$TiSe_2$ (the 1T trigonal arrangement of single layers produces generally semimetallic or semiconducting systems [20, 21]), CDW has been found with novel properties. 1T-$TiSe_2$ presents the hitherto unique feature of alternating sheets with a 3D helical stacking of intralayer charge modulation with the helical axis perpendicular to the layers [22]. Domains that are mirror images of each other, and cannot be brought together with only rotation operations, are found over the surface. The question of whether such a kind of chiral charge order can appear in a superconductor with CDW has not been addressed. Chiral symmetry is a particular example of the absence of space parity, a concept of fundamental importance for the Bardeen–Cooper–Schrieffer (BCS) theory. To our knowledge, the only known superconductor where chiral symmetry is at present debated is the p-wave superconductor Sr_2RuO_4 [23]. In Sr_2RuO_4, the chiral symmetry appears due to Cooper pair wavefunction phase winding at the superconducting transition, related to the particular

form of the p-wave order parameter. How superconductivity evolves out of a chiral electronic environment, however, is yet to be worked out. Here we do not resolve this question, but provide a significant advance by finding for the first time chiral charge order in a metallic compound, $2H\text{-}TaS_2$, which, in addition, superconducts below 1.75 K. We discuss chiral properties of CDW in this material and determine the superconducting density of states (DOS) from tunneling spectroscopy.

$2H\text{-}TaS_2$ single crystals were synthesized using an iodine transport method. Stoichiometric amounts of the elements were sealed under vacuum in a silica tube with a small amount of iodine ($5\,\text{mg cm}^{-3}$). The tube was then heated for a period of 15 days in a gradient furnace ($\approx 50\,^\circ\text{C}$ along the tube) with the mixture located in the high-temperature zone ($\approx 800\,^\circ\text{C}$). This synthesis yielded layered crystals some hundreds of μm in size that exhibit x-ray diffraction patterns corresponding to $2H\text{-}TaS_2$. For scanning tunneling microscopy (STM) measurements, we use an STM in a partially home-made dilution refrigerator setup described in detail elsewhere [24, 25]. The setup features the possibility to mount several very small (some tens of microns size) single crystals and change the position of the tip from one sample to the other *in situ*, at low temperatures. The gold tip can be moved to a sample of gold to clean and sharpen, and the energy resolution of the setup is of $15\,\mu$eV. Scanning was made at a constant current with tunneling conductances of about $0.1\,\mu$S and bias voltages usually below $10\,$mV. Several $2H\text{-}TaS_2$ samples were glued one by one using silver epoxy on an Au substrate, and measured at $100\,$mK. Samples were mechanically cleaved using scotch tape prior to the experiment. After cleaving, clean atomically flat surfaces are easily found, with the exposed surface composed of hexagons of the chalcogen atomic layer.

The STM topography at constant current of $2H\text{-}TaS_2$ taken at 100 mK is shown in figure 1(a). The hexagonal atomic S lattice is nicely observed, together with a remarkable triangular 3×3 charge modulation of wavelength 3 times the lattice constant. The Fourier transform of the whole image (right panel of figure 1(a)) shows that the CDW modulation is located at one-third the in-plane reciprocal lattice wavevectors, within experimental error of $\pm 1\%$. The CDW modulation leads to hexagons spanned by three vectors parallel to the three symmetry axes of the hexagonal atomic lattice, repeating itself in the topography. We identify two regions with different hexagonal patterns produced by the CDW modulation, marked by white rectangles in figure 1. In each region, within a given hexagon, the amplitude of the charge density along the three principal CDW vectors has an angular dependence, breaking sixfold rotational symmetry. The amplitude relationship between the three modulations varies when going from the upper left corner to the lower right one. In figure 1(b), we show representative topography profiles along the three CDW wavevectors. The CDW amplitude is highest along the red arrow direction in the upper left corner and along the green arrow direction in the lower right corner. The hexagonal pattern spanning the CDW modulation changes as a function of the position in the image, without any step or impurity cutting the image in two. Note that both parts cannot be transferred into each other by a simple rotation.

The angular dependence of the CDW modulation observed in the real space can be further characterized by making a detailed Fourier analysis. If we look at the Fourier transforms of the two different areas marked by rectangles in figure 1(a), we find that the amplitude of CDW Bragg peaks decrease clockwise (in R) and counter-clockwise (in L), respectively. The normalized amplitude relationships for, respectively, q_{CDW_1} (red), q_{CDW_2} (orange) and q_{CDW_3} (green) are 1–0.6–0.4 for the upper part of the image (R in figure 2(b)) and 0.6–0.8–1 for the bottom part of the image (L in figure 2(b)). This behavior is not followed by the intensity
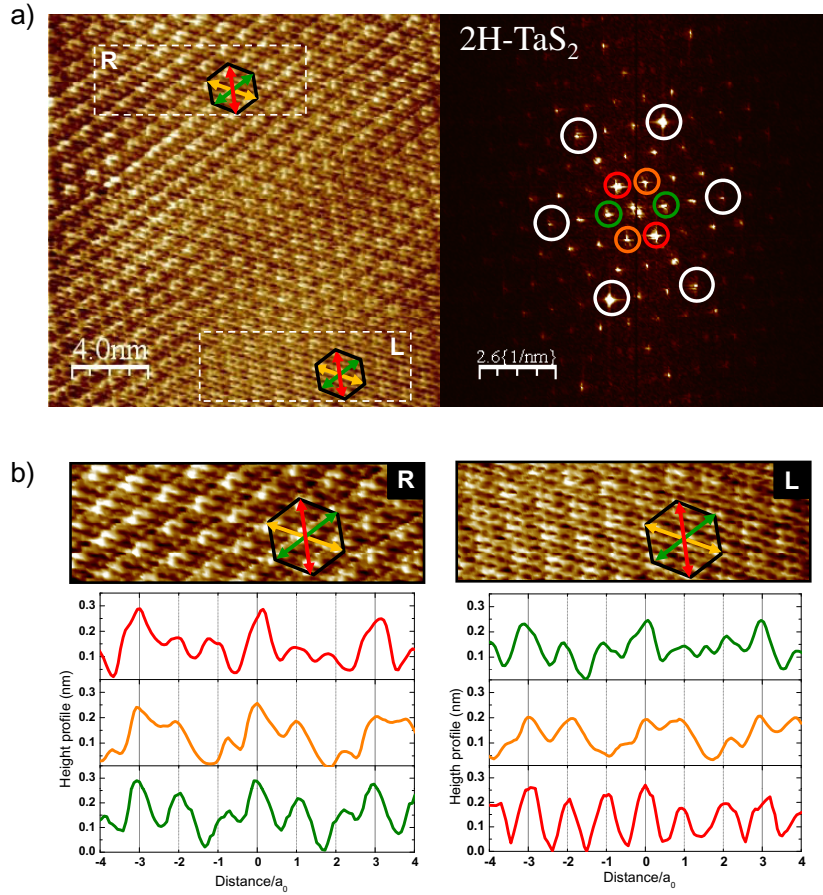
Figure 1. In (a), we show the STM topography at constant current made at 5 mV in 2H-TaS$_2$ at 100 mK (left panel), and its corresponding Fourier transform (right panel). White circles show Bragg peaks corresponding to the atomic S lattice, and colored circles those corresponding to the three CDW with reciprocal lattice vectors q_{CDW_1} (red), q_{CDW_2} (orange) and q_{CDW_3} (green). In (b), we show real space profiles taken along the three principal directions of the CDW modulations as marked by the arrows in (a) and zoomed-up images in the upper panels (corresponding to areas marked by dashed white rectangles in the top (R) and bottom (L) parts of the image). It gives a peculiar Moiré pattern where the height relationship changes from a rightwise rotating angular dependence to a leftwise rotating angular dependence in the same figure, without any defect or step observed in between.

changes of the lattice Bragg peaks and evidences the presence of chiral domains in the CDW of 2H-TaS$_2$.

The spatial distribution of the chiral domains can be imaged by further Fourier analysis. We first Fourier transform the whole real space image (shown in figure 1(a)), center the resulting Fourier image at the peak corresponding to CDW's component with highest amplitude in the upper left corner domain (q_{CDW_1}), filter the rest of the image out and re-transform into real space. This gives us the real space dependence of the CDW amplitude corresponding
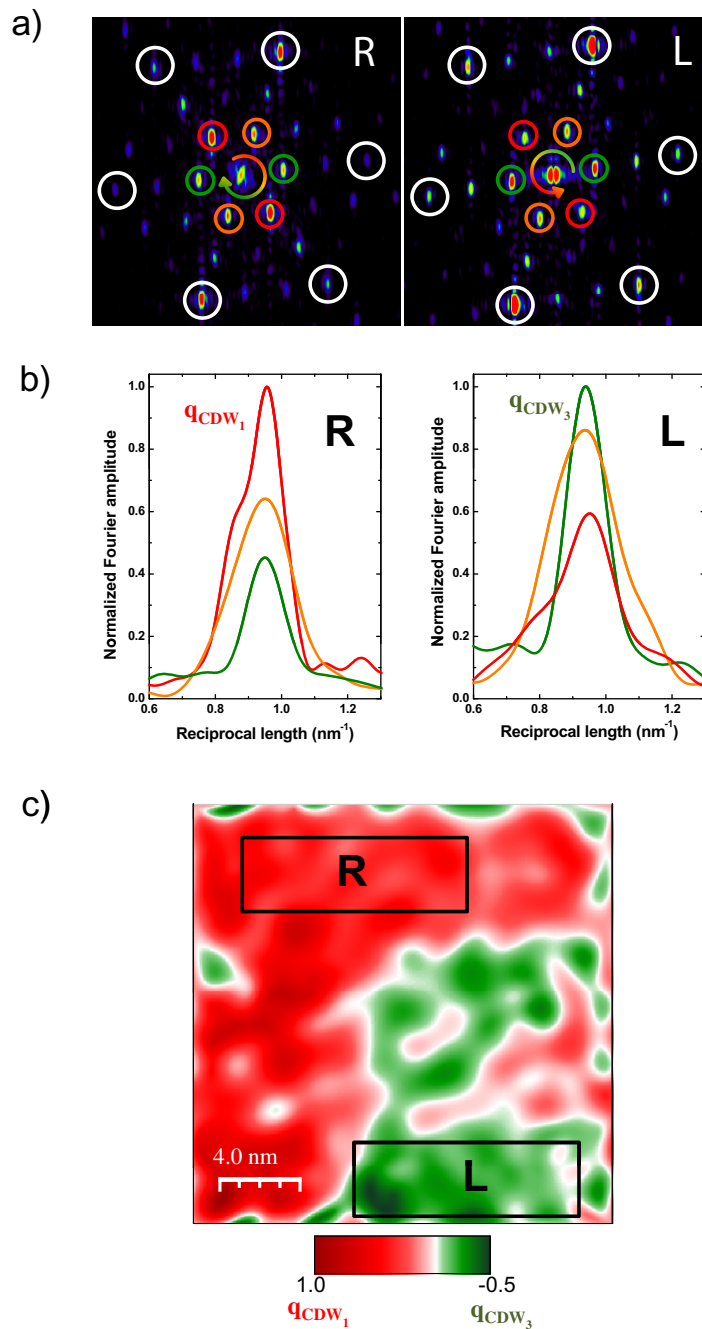
Figure 2. Fourier analysis of the CDW modulations of figure 1. In (a), we show the Fourier transform of the rectangles in the top (R) and bottom (L) areas of figure 1(a). Red, orange and green circles mark the Bragg peaks corresponding to each CDW modulation direction. The intensity of the peaks decreases, respectively, clockwise (R, from red to green in (c)) and anticlockwise (L, from green to red in (c)). In (b), profiles are normalized to one at the highest peak. In (c), we show a Fourier amplitude map highlighting the spatial distribution of the dominant CDW components. The map is obtained as described in the text and shows the difference between the amplitudes of q_{CDW_1} and q_{CDW_3} normalized by

Figure 2. (Continued) the highest value of the CDW_1 amplitude. The area where q_{CDW_1} has the highest amplitude is marked in red, and the area where q_{CDW_3} is highest is marked in green. White shows the boundary, where the size of both modulations is equal.

to the wavevector q_{CDW_1}. We then carry out the same procedure for the CDW modulation corresponding to q_{CDW_3} which has the highest amplitude in the lower right corner domain. Finally, we subtract both images [26], obtaining the map of the relative height between both modulations (figure 2(c)). We use red color for the area where q_{CDW_1} has the highest amplitude, and green color for the area where q_{CDW_3} has the highest amplitude (figure 2(c)). White color is used for the boundary, where both modulations have equal amplitude. The size of the areas with different CDW modulations is rather large, up to 10 nm, and their boundary is irregular.

The height of the atomic and CDW Fourier Bragg peaks measured in the transition metal dichalcogenides depends always on the direction. This is the result of the complex Moiré pattern, with very different hexagonal symmetry structures appearing in different positions, ubiquitously observed in these materials (see, e.g., [27, 28]). Calculating precisely the local DOS to obtain such patterns is a problem of great complexity. Tip–sample coupling, depending on the detailed band structure of the sample, and of the form and geometry of the tip, or defects, considerably shape the measured local DOS [29, 30]. For example, Moiré patterns of 2H-NbSe$_2$ have been widely discussed in the literature, and are related to different tip–sample coupling effects. In 2H-TaS$_2$, within the same image, without any change in the properties of the tip nor of the surface (i.e. without any step, defect or surface anomaly), the Moiré patterns change its symmetry properties, in a rather complex way, as shown in figures 1 and 2. This was first found in 1T-TiSe$_2$ [22] and, to the best of our knowledge, was never observed previously in any metallic 2H dichalcogenide compound. To explain such patterns, it is needed to consider out-of-plane decoupling of the three components of the CDW, which are combined in two different ways in different areas of the surface, giving chiral CDW order [22].

The microscopic origin of chiral charge arrangements is now under debate. Electronic interactions between planes (along c), which separate in-plane charge modulations through Coulomb interaction, can lead to a c-axis chiral modulation of the CDW [22]. More recently, it was shown that chiral charge order can also appear in relation to orbital order, which produces transversal polarization introducing phase shifts in the CDW [31]. The charge modulation observed in 2H-TaS$_2$ can be simulated by assuming that the intensity of the modulations corresponding to each CDW_i changes as a function of the out-of-plane stacking, or by phase shifting each component [22, 31]. For example, if we sum up three CDW components with $CDW_i(\mathbf{r}) = A_i \cos(q_{CDW_i} \mathbf{r})$ (with A_i being the amplitude of q_{CDW_i}) and two different amplitude relationships in two different areas, we obtain the image shown in figure 3(a). Qualitatively, the obtained shapes agree with the experimental image of the CDW (figure 3(b)).

All these observations, which are similar to those reported in the compound 1T-TiSe$_2$ [22], demonstrate that 2H-TaS$_2$ has a chiral modulation of its CDW. Note that 2H-TaS$_2$ is a metal that superconducts, but 1T-TiSe$_2$ is a semimetal with no report of superconducting correlations at ambient pressure [32]. Note also that in 1T-TiSe$_2$ the CDW modulation is located at two times the lattice constant, whereas in 2H-TaS$_2$ it is located at three times the lattice constant. The threefold in-plane symmetry with clockwise and counterclockwise domains appearing in the charge order features, is, however, similar. Furthermore, in 1T-TiSe$_2$, there is a c-axis modulation of the CDW [22], with periodicity two times the c-axis lattice constant. In

IOP Institute of Physics ❶ DEUTSCHE PHYSIKALISCHE GESELLSCHAFT
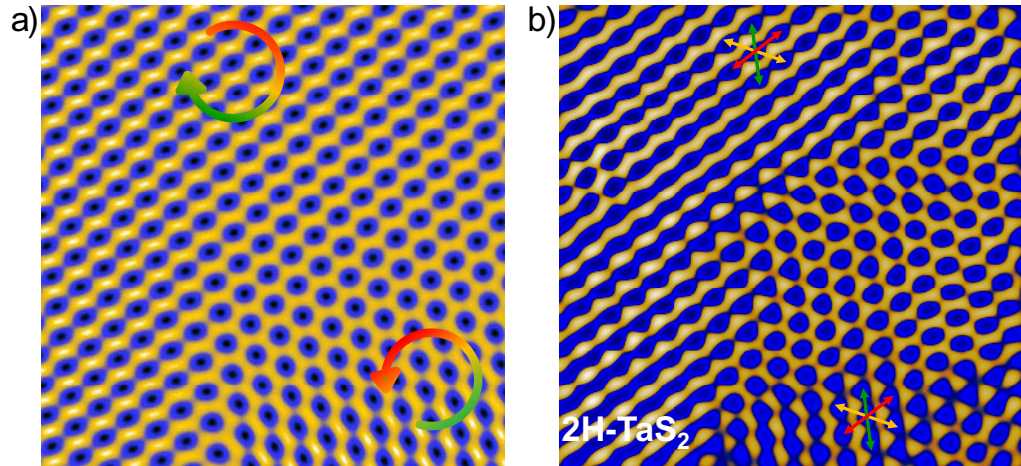
Figure 3. In (a) we show the charge modulation obtained by summing up three $CDW_i = A_i \cos(q_{CDW_i} \mathbf{r})$, using $A_1 = 1$, $A_2 = 0.6$, $A_3 = 0.3$ in the upper left corner's chiral domain (clockwise decrease of the amplitude of the CDW Fourier peaks as shown by the arrow) and $A_1 = 0.3$, $A_2 = 0.6$, $A_3 = 1$ in the lower right corner's chiral domain (counterclockwise decrease of the amplitude of the CDW Fourier peaks as shown by the arrow). These modulations give differently oriented oval-shaped patterns. In between, the difference between A_i are smoothly varied as a function of the position. As the difference in A_i becomes smaller, a circularly shaped pattern is visible. Panel (b) shows the CDW modulation observed in the experiment. Atomic lattice modulations are removed from figure 1 by Fourier transform filtering. Oval-shaped patterns are observed in the two chiral domains, with more round circular patterns along the chiral domain wall. Arrows indicate main CDW modulation directions, as in figure 1. In both figures, the color goes continuously from dark blue for the highest charge density to white for the lowest charge density.

2H-TaSe$_2$, interlayer separation is highest among the 2H series (it is continuously decreasing from 2H-TaSe$_2$, 2H-TaS$_2$, 2H-NbSe$_2$ and is smallest in 2H-NbS$_2$, where no CDW is observed); the three coexisting CDWs lead to a reduction of the crystal symmetry from hexagonal to orthorhombic [33]. In 2H-NbSe$_2$, as discussed above, no chiral CDW has been reported, in spite of having been very extensively studied by many different groups. It could be that 2H-TaS$_2$ lies in between both cases, being sufficiently 2D to present de-coupling of CDW modulations, but not enough to show structural transition or to destroy superconductivity through a too strong destruction of the Fermi surface by the CDW gap opening.

The superconducting tunneling conductance of 2H-TaS$_2$ measured at 100 mK is shown in figure 4. The tunneling conductance remains flat until around 0.15 mV, where it starts increasing continuously until 0.4 mV, where the quasiparticle peak is located. Such a feature is found over large parts of the surface, and we could not, until now, observe changes related to the domains of the chiral CDW modulation. The behavior is instead reminiscent of the compounds 2H-NbSe$_2$ and 2H-NbS$_2$, where a distribution of values of the superconducting gap, starting also roughly at half the maximal gap value, is found. In the latter compounds, however, two clear features are seen in the tunneling conductance, which show up as two peaks in the derivative
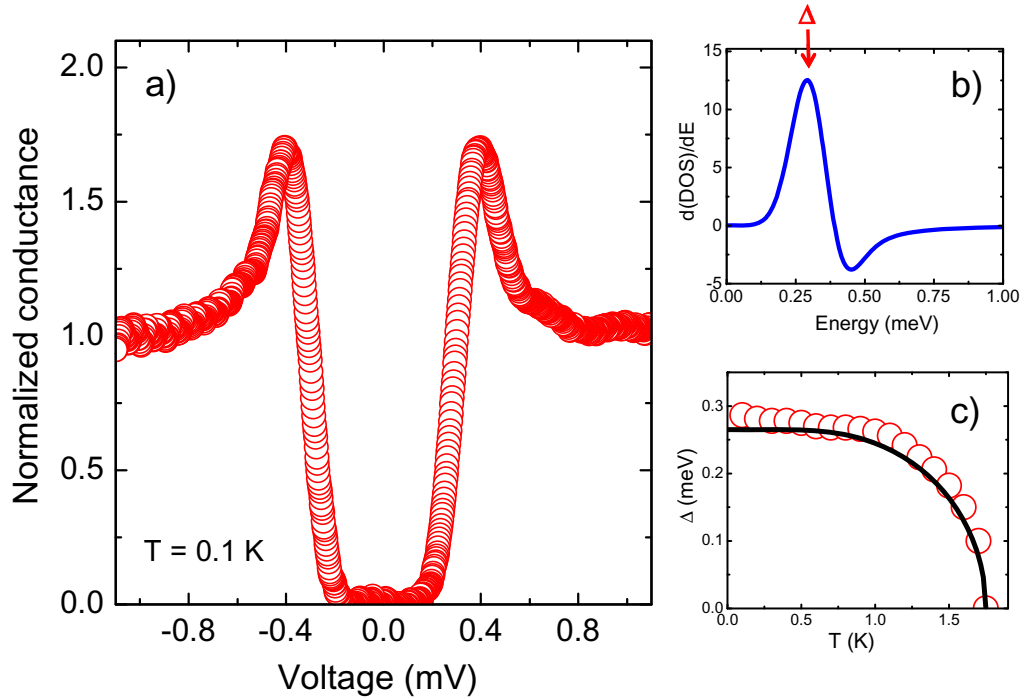
Figure 4. (a) Normalized tunneling conductance curve obtained in 2H-TaS$_2$ at 0.1 K (the conductance σ at 1 mV is 1.7 μS). In (b), we show the derivative of the associated local DOS, which has been obtained by de-convoluting the temperature from the tunneling conductance. The derivative has a peak at $\Delta = 0.28$ meV. In (c), we show the temperature dependence of Δ (red circles) and expectation from BCS theory (black line) with $T_c = 1.75$ K.

of the corresponding DOS [9, 16]. These features are due to the two band superconducting properties characteristic of these compounds. Here, the derivative of the DOS (obtained by de-convoluting the temperature, as shown in [9]) shows only one broad peak centered at $\Delta = 0.28$ meV (figure 4), which evolves until $T_c = 1.75$ K following roughly BCS theory. The value we found for Δ is close to, although somewhat larger than, the value expected within BCS theory, $\Delta = 1.76 k_B T_c = 0.265$ meV. Thus, the superconducting gap of 2H-TaS$_2$ has a significant anisotropy, and the two gap features characteristic of 2H-NbSe$_2$ and 2H-NbS$_2$ are, if they exist at all, less clearly resolved in the superconducting DOS.

Our results establish that, in 2H-TaS$_2$, chiral CDW properties coexist with superconductivity. Possible consequences could be related to those found in the context of other superconductors with broken space inversion symmetry. For example, in a superconductor with broken space parity and strong spin–orbit coupling (spin–orbit coupling is strong in 2H-TaS$_2$ as discussed in [34]), the twofold electronic spin degeneracy may be lifted and spin structured Cooper pairs could appear [35–39]. The form and size of the superconducting gap can be, under such conditions, peculiar, with nodes along some directions, but it can also be fully opened [23, 40]. In 2H-TaS$_2$, the present observation of an opened somewhat anisotropic gap, similar to those found in related materials, makes it difficult to discuss the possible influence of broken space parity in the superconducting properties. Characterization of superconductivity in the other system of the series, 2H-TaSe$_2$ [34], observation of the vortex lattice in both compounds

IOP Institute of Physics ⏀ DEUTSCHE PHYSIKALISCHE GESELLSCHAFT

and a closer look at superconductivity in related CDW materials should bring about further advances.

In summary, we have observed a chiral CDW in a metallic and superconducting compound, $2H\text{-}TaS_2$, and provide measurements of its superconducting DOS. We could not establish an influence of broken space parity through a helical electronic structure on the superconducting DOS, but the mere presence of both phenomena in the same material calls for more work on this and similar compounds.

Acknowledgments

References

[1] Anderson P W and Blount E I 1965 Symmetry considerations on martensitic transformations: 'ferroelectric' metals? *Phys. Rev. Lett.* **14** 217

[2] Kiss T, Yokoya T, Chainany Aa, Shin S, Hanaguri T, Nohara M and Takagi H 2007 Charge-order-maximized momentum-dependent superconductivity *Nature Phys.* **3** 720–5

[3] Rossnagel K, Seifarth O, Kipp L, Skibowski M, Voß D, Krüger P, Mazur A and Pollmann J 2001 Fermi surface of $2H\text{-}NbSe_2$ and its implications on the charge-density-wave mechanism *Phys. Rev.* B **64** 235119

[4] Castro Neto A H 2001 Charge density wave, superconductivity and anomalous metallic behavior in 2d transition metal dichalcogenides *Phys. Rev. Lett.* **86** 4382–5

[5] Suderow H, Tissen V G, Brison J P, Martinez J L and Vieira S 2005 Pressure induced effects on the Fermi surface of superconducting $2H\text{-}NbSe_2$ *Phys. Rev. Lett.* **95** 117006

[6] Hess H F, Robinson R B and Waszczak J V 1990 Vortex-core structure observed with a scanning tunneling microscope *Phys. Rev. Lett.* **64** 2711

[7] Gygi F and Schluter M 1990 Angular band structure of a vortex line in a type-II superconductor *Phys. Rev. Lett.* **65** 1820

[8] Hayashi N, Ichioka M and Machida K 1996 Star-shaped local density of states around vortices in a type-II superconductor *Phys. Rev. Lett.* **77** 4074

[9] Guillamon I, Suderow H, Vieira S, Cario L, Diener P and Rodiere P 2008 Superconducting density of states and vortex cores of $2H\text{-}NbS_2$ *Phys. Rev. Lett.* **101** 166407

[10] Wilson J A, DiSalvo F J and Mahajan S 1975 Charge-density waves and superlattices in the metallic layered transition metal dichalcogenides *Adv. Phys.* **24** 117

[11] Corcoran R, Meeson P, Onuki Y, Probst P A, Springford M, Takita K, Harima H, Guo G Y and Gyoffry B L 1994 Quantum oscillations in the mixed state of the type-II superconductor $2H\text{-}NbSe_2$ *J. Phys.: Condens. Matter* **6** 4479–92

[12] Johannes M D, Mazin I I and Howells C A 2006 Fermi-surface nesting and the origin of the charge-density wave in $NbSe_2$ *Phys. Rev.* B **73** 205102

[13] Ge Y and Liu A Y 2010 First principles investigation of the charge-density-wave instability in $1T\text{-}TaSe_2$ *Phys. Rev.* B **82** 155133

[14] Sacks W, Roditchev D and Klein J 1998 Voltage-dependent STM image of a charge density wave *Phys. Rev.* B **57** 13118–31

[15] Boaknin E *et al* 2003 Heat conduction in the vortex state of $NbSe_2$: evidence for multiband superconductivity *Phys. Rev. Lett.* **90** 117003

[16] Rodrigo J G and Vieira S 2004 STM study of multiband superconductivity in NbSe$_2$ using a superconducting tip *Physica* C **404** 306

[17] Fletcher J D, Carrington A, Diener P, Rodiére P, Brison J P, Prozorov R, Olheiser T and Giannetta R W 2007 Penetration depth study of superconducting gap structure of 2H-NbSe$_2$ *Phys. Rev. Lett.* **98** 057003

[18] Noat Y, Cren T, Debontridder F, Roditchev D, Sacks W, Toulemonde P and San Miguel A 2010 Signatures of multigap superconductivity in tunneling spectroscopy *Phys. Rev.* B **82** 014531

[19] Kacmarcik J, Prbulova Z, Marcenat C, Klein T, Rodiere P, Cario L and Samuely P 2010 Specific heat measurements of a superconducting 2H-NbS$_2$ single crystal in an external magnetic field: energy gap structure *Phys. Rev.* B **82** 014518

[20] Bulaevskii L N 1976 Superconductivity and electronic properties of layered compounds *Sov. Phys.—Usp.* **18** 514

[21] DiSalvo F J, Moncton D E and Waszcak J V 1976 Electronic properties and superlattice formation in the semimetal TiSe$_2$ *Phys. Rev.* B **14** 4321

[22] Ishioka J, Liu Y H, Shimatake K, Kurosawa T, Ichimura K, Toda Y, Oda M and Tanda S 2010 Chiral charge-density waves *Phys. Rev. Lett.* **105** 176401

[23] Mackenzie A P and Maeno Y 2003 The superconductivity of Sr$_2$RuO$_4$ and the physics of spin–triplet pairing *Rev. Mod. Phys.* **75** 657

[24] Rodrigo J G, Suderow H, Vieira S, Bascones E and Guinea F 2004 Superconducting nanostructures fabricated with the scanning tunnelling microscope *J. Phys.: Condens. Matter* **16** 1151

[25] Suderow H, Guillamon I and Vieira S 2011 Compact very low temperature scanning tunneling microscope with mechanically driven horizontal linear positioning stage *Rev. Sci. Instrum.* **82** 033711

[26] Zelkjovic I *et al* 2011 STM imaging of inversion-symmetry-breaking structural distortion in the Bi-based cuprate superconductors arXiv:1104.4342

[27] Coleman R V, Giambattista B, Hansma P K, Johnson A, McNairy W W and Slough C G 1988 Scanning tunneling microscopy of charge density waves in transition metal chalcogenides *Adv. Phys.* **37** 559–644

[28] Giambattista B, Johnson A, Coleman R V, Drake B and Hansma P K 1988 Scanning tunneling microscopy of charge density waves in transition metal chalcogenides *Phys. Rev.* B **37** 2741

[29] Tersoff J and Hamann D R 1983 Theory and application for the scanning tunneling microscope *Phys. Rev. Lett.* **50** 1998–2001

[30] Guillamon I, Suderow H, Guinea F and Vieira S 2008 Intrinsic atomic-scale modulations of the superconducting gap of 2H-NbSe$_2$ *Phys. Rev.* B **77** 134505

[31] van Wezel J 2011 Chirality and orbital order in charge density waves arXiv:1106.1930v1

[32] Kusmartseva A F, Sipos B, Berger H, Forro L and Tutis E 2009 Pressure induced superconductivity in pristine 1T-TiSe$_2$ *Phys. Rev. Lett.* **103** 236401

[33] Littlewood P B and Rice T M 1982 Theory of the splitting of discommensurations in the charge-density-wave state of 2H-TaS$_2$ *Phys. Rev. Lett.* **48** 27

[34] Rossnagel K and Smith N V 2007 Spin–orbit splitting, Fermi-surface topology, and charge-density-wave gapping of 2H-TaSe$_2$ *Phys. Rev.* B **76** 073102

[35] Edelstein V M 1995 Magnetoelectric effect in polar superconductors *Phys. Rev. Lett.* **75** 2004

[36] Schnyder A P and Ryul S 2010 Topological phases and flat surface bands in superconductors without inversion symmetry arXiv:1011.1438v1

[37] Bauer E *et al* 2010 Unconventional superconductivity in weakly correlated, non-centrosymmetric Mo$_3$Al$_2$C arXiv:1007.0420v1

[38] Gor'kov L P and Rashba E I 2001 Superconducting 2D system with lifted spin degeneracy: mixed singlet–triplet state *Phys. Rev. Lett.* **87** 037004

[39] Samokhin K V and Mineev V P 2008 Gap structure in noncentrosymmetric superconductors *Phys. Rev.* B **77** 104520

[40] Suderow H, Crespo V, Guillamon I, Vieira S, Servant F, Lejay P, Brison J P and Flouquet J 2009 A nodeless superconducting gap in Sr$_2$RuO$_4$ from tunneling spectroscopy *New J. Phys.* **11** 093004